









RESEARCH ARTICLE

Obesogenic diet leads to luminal overproduction of the complex IV inhibitor H₂S and mitochondrial dysfunction in mouse colonocytes

Thomas Guerbette¹  | Martin Beaumont²  | Mireille Andriamihaja³  |
Vincent Ciesielski^{1,4}  | Jean-Baptiste Perrin¹ | Régis Janvier¹ | Gwénaëlle Randuineau¹ |
Patricia Leroyer¹ | Olivier Loréal¹  | Vincent Rioux^{1,4}  | Gaëlle Boudry¹  |
Annaïg Lan^{1,3} 

¹Institut Numecan, INRAE, INSERM, Univ Rennes, Rennes, France

²GenPhySE, Université de Toulouse, INRAE, ENVT, Castanet-Tolosan, France

³UMR PNCA, AgroParisTech, INRAE, Université Paris-Saclay, Palaiseau, France

⁴Institut Agro, Univ Rennes, INRAE, INSERM, NuMeCan, Rennes, France

Correspondence

Annaïg Lan, UMR PNCA, AgroParisTech, INRAE, Université Paris-Saclay, Palaiseau, France.
Email: annaig.lan@agroparistech.fr

Funding information

Région Bretagne (Region Brittany), Grant/Award Number: #300000592

Abstract

Obesity is characterized by systemic low-grade inflammation associated with disturbances of intestinal homeostasis and microbiota dysbiosis. Mitochondrial metabolism sustains epithelial homeostasis by providing energy to colonic epithelial cells (CEC) but can be altered by dietary modulations of the luminal environment. Our study aimed at evaluating whether the consumption of an obesogenic diet alters the mitochondrial function of CEC in mice. Mice were fed for 22 weeks with a 58% kcal fat diet (diet-induced obesity [DIO] group) or a 10% kcal fat diet (control diet, CTRL). Colonic crypts were isolated to assess mitochondrial function while colonic content was collected to characterize microbiota and metabolites. DIO mice developed obesity, intestinal hyperpermeability, and increased endotoxemia. Analysis of isolated colonic crypt bioenergetics revealed a mitochondrial dysfunction marked by decreased basal and maximal respirations and lower respiration linked to ATP production in DIO mice. Yet, CEC gene expression of mitochondrial respiration chain complexes and mitochondrial dynamics were not altered in DIO mice. In parallel, DIO mice displayed increased colonic bile acid concentrations, associated with higher abundance of Desulfovibrionaceae. Sulfide concentration was markedly increased in the colon content of DIO mice. Hence, chronic treatment of CTRL mouse colon organoids with sodium sulfide provoked mitochondrial dysfunction similar to that observed in vivo in DIO mice while acute exposure of isolated mitochondria from CEC of CTRL mice to sodium sulfide diminished

Abbreviations: CEC, colonic epithelial cells; DIO, diet-induced obesity; ECAR, extracellular acidification rate; ETC, electron transport chain; FAME, fatty acid methyl esters; LBP, lipopolysaccharide-binding protein; OCR, oxygen consumption rate; OXPHOS, oxidative phosphorylation; ROS, reactive oxygen species; SCFA, short-chain fatty acid.

Gaëlle Boudry and Annaïg Lan contributed equally.

This is an open access article under the terms of the [Creative Commons Attribution-NonCommercial-NoDerivs](https://creativecommons.org/licenses/by-nc-nd/4.0/) License, which permits use and distribution in any medium, provided the original work is properly cited, the use is non-commercial and no modifications or adaptations are made.

© 2023 The Authors. *The FASEB Journal* published by Wiley Periodicals LLC on behalf of Federation of American Societies for Experimental Biology.

complex IV activity. Our study provides new insights into colon mitochondrial dysfunction in obesity by revealing that increased sulfide production by DIO-induced dysbiosis impairs complex IV activity in mouse CEC.

KEYWORDS

high fat diet, intestine, obesity, microbiota, mitochondria

1 | INTRODUCTION

Obesity and overweight are spreading worldwide, notably due to obesogenic diet consumption, containing high-fat/sugar levels. They cause the death of 4 million people each year due to complications, such as cardiovascular diseases or cancers, which are associated with low-grade inflammation.^{1,2} Animal models of diet-induced obesity (DIO) have reported that excess body fat was associated with metabolic endotoxemia,¹ alterations of the gut luminal environment,³ and intestinal permeability,⁴ observed in mouse colon^{3,5} and in the small intestine in human obesity.⁶ Colonic homeostasis relies on the cross talk between the microbiota, the intestinal epithelium, and the host immune system. Hence, the intestinal epithelium acts as a barrier, made of intestinal epithelial cells associated with each other by tight junctions and of protective mucus layer. Active transport of water and electrolytes, rapid epithelial cell renewal, and maintaining of intestinal barriers are high-energy consuming processes. This energy is mainly supplied by mitochondria that produce energy via oxidative phosphorylation (OXPHOS).⁷ Yet, mitochondrial dysfunction, defined as any mechanism that reduces the efficiency of OXPHOS and leads to decreased levels of cellular ATP, weakens intestinal epithelial barrier function.⁷ Indeed, uncoupling OXPHOS in intestinal T84 cells provoked an increase in *Escherichia coli* translocation.^{8–10} To date, some signs of energetic defects in colonic epithelial cells (CEC) of DIO mice have been observed in several studies. DIO mice presented swollen mitochondria¹¹ associated with decreased amounts of ATP in CECs,¹² or reduced expression of genes encoding electron transport chain (ETC) subunits.^{12,13} Decreased mitochondrial pyruvate dehydrogenase activity and elevated intracellular lactate levels in CEC also suggest a metabolic shift toward glycolysis in DIO.¹³ Nevertheless, no study has performed a complete functional evaluation of mitochondrial function of CEC in DIO mice so far. Moreover, the mechanisms whereby obesogenic diet consumption could lead to mitochondrial dysfunction are unclear. It is believed that mitochondrial dysfunction in DIO could be a downstream consequence of increased dietary fatty acid β -oxidation that generates reactive oxygen species (ROS). Indeed, treating CEC with palmitic acid in vitro induces mitochondrial dysfunction and ROS generation.^{13,14} Yet, the colon is not the

preferential site of dietary lipid absorption, weakening this hypothesis. Moreover, diet composition alters the luminal environment composition, especially the quantity and/or variety of diet-derived bacterial metabolites,¹⁵ some of which are detrimental or beneficial to CEC according to their concentration, by acting on mitochondria.⁷

Thus, because of the central role of mitochondrial function in the maintenance of intestinal epithelium homeostasis, we aimed to better characterize the mitochondrial function of CEC in DIO mice and to uncover the possible role of microbiota dysbiosis and alteration of the colonic luminal environment.

2 | MATERIALS AND METHODS

2.1 | Animal experiment

Animal procedures were performed in accordance with French law and approved by the Comité Rennais d'Ethique en Expérimentation Animale and by the Ministère de l'Enseignement Supérieur et de la Recherche (APAFIS# 22076-2019091911225127 v4). Thirty-two 4-week-old C57BL/6J male mice, from Janvier Labs (Le Genest-Saint-Isle, France) were housed in a group of 4 per cage at 20°C with a 12:12 h light–dark cycle. After an acclimation week with a chow diet (5% kcal fat, Envigo, Gannat, France), animals were divided into two groups and received ad libitum for 22 weeks either a control diet (CTRL, D12328; 10% kcal fat, Research Diets, New Brunswick, NJ, $n = 17$) and plain water or an obesogenic diet (DIO, D12331, 58% kcal fat, Research Diets, $n = 15$) and drinking water supplemented with a mix of carbohydrates (45% sucrose and 55% fructose) at 42 g/L. Animals were euthanized through intracardiac puncture following sedation by isoflurane. Four centimeters of the proximal colon were maintained in cold Hanks' Balanced Salt Solution (HBSS, 14170112, Gibco, Illkirch, France) until colon crypt isolation, 1 cm maintained in Krebs buffer for immediate permeability assay in Ussing chamber. Luminal colonic content was removed and snap frozen in liquid nitrogen and stored at -80°C for further microbiota and metabolomic analysis. For the sulfide assay, colonic content was homogenized in deoxygenated PBS 1:10 (weight/volume) using the tissue homogenizer

Minilys (Bertin-corp, P000673-MLYS0-A, Rockville, USA). Deoxygenated PBS was obtained after a 48 h incubation into an anaerobic enclosure. Blood samples were left on ice for 2 h and then centrifugated at 240g for 10 min. Serum was aliquoted and stored at -80°C .

For complex IV activity assay on isolated mitochondria, 5 male C57BL/6J mice from Janvier Labs were acclimated for a week with a chow diet and then received the CTRL diet ad libitum for 2 weeks before euthanasia.

2.2 | Evaluation of diet-induced obesity

Adiposity visceral index was obtained through the sum of abdominal, peritoneal, and epididymal fat pad weights related to body weight and expressed as a percentage. To determine endotoxemia, the concentration of lipopolysaccharide-binding protein (LBP) from serum samples, diluted at 1:75, was measured by ELISA following the manufacturer's instruction (EK1274, Tebubio, Le Perray-en-Yvelines, France). Cholesterol and triglycerides in serum were measured in the Biochemistry Department at the Rennes University Hospital.

2.3 | Colonic permeability

Colonic permeability was measured using Ussing chambers as previously described¹⁶ using FD4 (FD4, Sigma-Aldrich, Saint-Quentin-Fallavier, France) as a permeability marker.

2.4 | Colonic crypt isolation

Isolation of colonic crypts was performed as previously described¹⁷ and consisted in incubating colon in prewarmed 20 mM ethylenediaminetetraacetic acid/HBSS solution (pH = 8), for 30 min at 37°C . To allow crypt isolation, the colon was hardly agitated in cold HBSS and isolated crypts were counted under an inverted microscope. After the addition of 10% fetal bovine serum (SH30066.03, HyClone, GE Healthcare, Chicago, USA) isolated crypts were centrifuged for 5 min at 200g and resuspended into Advanced Dulbecco's Modified Eagle Medium (DMEM)/F12 (ADF, 12634010, Gibco) supplemented with 1% penicillin/streptomycin and 1% 4-(2-hydroxyethyl)-1-piperazineethanesulfonic acid (15630106, Gibco), to stabilize pH. Isolated crypts were then immediately used for metabolic analyses, ROS detection, and fatty acid β -oxidation while the remaining crypts were centrifugated, 350g for 5 min, and resuspended in lysis buffer RA1 (Macherey-Nagel, Hoerd, France) and stored at -80°C for further RNA or DNA extraction.

2.5 | qPCR and evaluation of mitochondrial mass in isolated colonic crypts

Isolated colonic crypt RNAs were extracted following the manufacturer's protocol (740955.250, Macherey-Nagel) and assayed using a Spectrometer ND-1000 (Nanodrop). cDNA was synthesized using the High-Capacity cDNA Reverse Transcription Kit (4368814, ThermoFisher Scientific, Illkirch, France) from 1 μg RNA for each sample in 20 μL of nuclease-free water. cDNAs were diluted 1:10 in nuclease-free water (10977035, ThermoFisher Scientific) and were used for real time-quantitative PCR (RT-qPCR) on 384-well plates filled with 2 μL of cDNA samples, 5 μL of PowerSYBR green PCR Master Mix kit (4368813, ThermoFisher Scientific), 0.2 μL of each primer at 10 μM (Eurogentec), and 2.6 μL of nuclease-free water. The expression of the genes of interest was analyzed using the $2^{-\Delta\Delta\text{Ct}}$ method with Hypoxanthine Phospho Ribosyl Transferase 1 (*Hprt1*) as a housekeeping gene. For the evaluation of mitochondrial mass, total DNA was extracted from isolated colonic crypts using the Qiagen DNeasy Blood & Tissue kit (69504, Qiagen, Les Ulis, France) following the manufacturer's instructions. Mitochondrial content was assayed by qPCR as described above by amplifying a portion of mtDNA (mt-Co1) and normalized by amplifying a nuclear fraction (haptoglobine). The primer sequences are available on demand.

2.6 | Extracellular flux analysis of isolated colonic crypts

Metabolic analysis of isolated colonic crypts was performed with the extracellular flux analyzer Seahorse XFe24 (Agilent Seahorse XF technology). Prior to the experiment, a Seahorse cell culture plate from the seahorse XFe24 Fluxpak (102340-100, Agilent, Les Ulis, France) was coated with 50 μL per well of 1:10 Matrigel (Corning® Matrigel® Growth Factor Reduced Basement Membrane Matrix, 354230, Boulogne-Billancourt, France) diluted in the Seahorse medium (Agilent, 102353-100) for 1 h at room temperature (RT) and stored at 4°C overnight. Cartridge plate was hydrated with calibrate buffer and incubated overnight at 37°C . One hour before crypt seeding, the plate was warmed up at RT, diluted Matrigel was removed and wells were washed twice with 50 μL of Seahorse medium. Fifty microliters of Seahorse complete medium, containing 1 mM pyruvate, 2 mM L-glutamine, and 10 mM glucose, were added to each well. Isolated crypts in ADF were centrifugated, 300g for 5 min, and resuspended in Seahorse complete medium (500 crypts/50 μL). Fifty

microliters of crypt suspension were seeded per well of the 24-Seahorse culture plate completed with 450 μ L of warm Seahorse complete medium. Plate was then incubated for 45 min at 37°C in a non-CO₂ incubator, to de-gas the plate, while the machine was calibrated. Mitochondrial function analysis was performed using the Cell Mito Stress Test kit (103015-100, Agilent) at the following final concentrations: Oligomycin (2 μ M), an inhibitor of ATP synthase to determine the proton leak, FCCP (0.5 μ M), to measure the maximal respiration, and Antimycin A and Rotenone (0.5 μ M), to determine the nonmitochondrial respiration. Three measurement cycles of oxygen consumption rate (OCR) and extracellular acidification rate (ECAR) were performed at basal state before any injection, and at metabolic stressed state, stimulated by the FCCP injection. Measures consisted of cycles of 3 min mix, 2 min wait, and 3 min measurement after each injection. At the end of the assay, cells were fixed and stained with Hoechst 33258 (H3569, ThermoFisher Scientific), which stains double-strand DNA, for normalization.

2.7 | Total lipid assay on colonic crypts and caecum contents

Colonic crypts and caecum contents were weighed and sonicated in 1 mL of PBS. One hundred micrograms of C17:0 were added to each sample as an internal standard for quantification. Lipid extraction was performed by adding 4 mL of a mix of 3:2 (volume:volume) hexane/isopropanol, acidified with 600 μ M HCl, in each sample. After a 15 min agitation at room temperature, samples were centrifugated at 1000g for 10 min, and the upper phase, which contains lipids, was transferred to a new tube containing 150 mM NaCl in order to rinse the organic phase. The tubes were vigorously shaken and centrifugated at 1000g for 3 min. Hexane was then totally evaporated with nitrogen flow at 55°C. Transmethylation of fatty acids from total lipids was then performed by adding 500 μ M NaOH for 20 min at 70°C to allow saponification, and then adding 1.5 M BF₃ in methanol for 20 min at 70°C, to allow methylation. To isolate fatty acid methyl esters (FAME), 150 mM NaCl and pentane were added to each tube. The upper phase containing the FAME into pentane was transferred to a new tube and evaporated as previously described. Finally, FAME were resuspended in hexane, and 1 μ L of each sample was injected. Total FAME were analyzed using an Agilent 7890 N gas chromatograph coupled to a 5975C mass spectrometry detector (Agilent) as previously described.¹⁸ The total fatty acids quantified by this method and expressed as μ g/mg of caecum content or

μ g/mg of colonic crypt cells were used as a proxy of total lipid content.

2.8 | Fatty acid β -oxidation assay of isolated colonic crypts

Isolated colonic crypts were centrifugated at 300g for 5 min, resuspended in 1:4 (volume/volume) Matrigel diluted in William's medium (A12176-01, Gibco) and 40 μ L per well were seed on a 96 well plate. Another plate, plated in the same condition, was used to normalize DNA content with Hoechst staining. The plate for fatty acid β -oxidation assay was incubated at 37°C, 5% CO₂ to allow the Matrigel to solidify. William's medium containing 1% BSA, 100 μ M palmitic acid (P5585, Sigma-Aldrich), 1 mM L-Carnitine (C0283, Sigma-Aldrich), and 0.05 μ Ci/mL [U-¹⁴C]-palmitic acid (NEC534050UC, Perkin-Elmer) was then added to each well (100 μ L), and the plate was incubated for 3 h in a 37°C, 5% CO₂ incubator. Then, 1 M perchloric acid was added to each well (100 μ L) and incubated at 37°C for 5 min to allow palmitic acid precipitation. The content of each well was then centrifugated at 2000g for 10 min. Supernatants containing radioactive metabolites from palmitic acid β -oxidation were collected and transferred to 4 mL of scintillation fluid. A liquid scintillation analyzer (TRI-CARB 4910TR, Perkin-Elmer) recorded the disintegrations per minute of each sample.

2.9 | ROS detection in mouse-isolated colonic crypts

Three thousand isolated colonic crypts were centrifugated at 300g for 5 min and resuspended in 10 μ M H₂DCFDA (D399, ThermoFisher Scientific), to detect peroxides, or in 10 μ M MitoSOX (M36008, ThermoFisher Scientific), to detect mitochondrial superoxide anions, both diluted in PBS. Crypts were incubated for 30 min at 37°C and protected from light. Then they were centrifugated at 300g for 5 min and resuspended in PBS. ROS were detected by measuring DCF fluorescence intensity at ex485/em590 and MitoSOX at ex520/em590 using the POLARstar Omega microplate reader (BMG Labtech). Results were normalized by measuring the Hoechst fluorescence intensity.

2.10 | Colonic content microbiota composition analysis

Bacterial DNA was extracted from colonic content samples using the ZR fecal DNA Miniprep kit (D6010,

Zymo Research, Irvine, USA). The V3-V4 region of 16S rRNA gene was amplified using the following primers: CTTTCCTACACGACGCTCTTCCGATCTACTCCTACGGGAGGCAGCAG(V3F) and GGAGTTCAGACGTGTGCTCTTCCGATCTTACCAGGGTATCTAATCC(V4R), Taq Phusion (New England Biolabs, Évry-Courcouronnes, France) and dNTP (New England Biolabs) for 25 cycles (10s to 98°C, 30s at 45°C, and 45s at 72°C). Agarose gel electrophoresis was performed to verify amplicon purity before sequencing using Illumina MiSeq technology, performed at the Genotoul GeT-PlaGe platform (Toulouse, France). The raw sequences were analyzed using the FROGS bioinformatics pipeline to obtain the richness (number of species) and β -diversity parameters as well as the relative abundances of the different taxa for each sample as already described.¹⁹ 16S sequence fasta file of the colonic microbiota data and associated metadata are available on the following link: <https://doi.org/10.57745/GJXAGJ>.

2.11 | Metabolome analysis of colonic contents by ¹H-NMR

Metabolome analysis was performed by using ¹H nuclear magnetic resonance (NMR) spectroscopy as described before.²⁰ Briefly, colonic content (approximately 50 mg) was homogenized in phosphate buffer (pH 7) prepared in D₂O and containing the internal standard trimethylsilylpropanoic acid (1 mM) using a FastPrep Instrument (MP biomedical, Irvine, CA). After centrifugation at 12 000g for 10 min at 4°C, the supernatant was collected. The pellet was resuspended in phosphate buffer, homogenized, and centrifuged as described above. The two supernatants were mixed together and centrifuged twice at 18 000g for 30 min at 4°C. Finally, the resulting supernatant was transferred into a 5 mm NMR tube. All NMR spectra were obtained with a Carr-Purcell-Meiboom-Gill sequence on an Avance III HD NMR spectrometer and analyzed on the MetaboHUB-MetaToul-AXIOM metabolomics platform (Toulouse, France). Raw spectra were processed in R (4.2.0) with the ASICS package (2.12.0)²¹ for baseline correction, normalization by total area, and bucketing (0.01 ppm bins). Metabolites were identified by comparison with the spectra of pure compounds and are presented in Table S1. For each metabolite, a bucket corresponding to a peak nonoverlapping with peaks from other metabolites was selected for quantification. The relative concentration of each metabolite was calculated by dividing the area under the curve of the corresponding bucket by the mean area of the same bucket in the CTRL group.

2.12 | Prediction of the functional potential of the colon microbiota

PICRUSt2 was used for the prediction of metagenome functions²² as implemented in FROGS²³ according to the guidelines. The 16S rRNA gene sequences of operational taxonomic unit (OTU) identified by FROGS were placed in the PICRUSt2 reference tree with *epa-ng*. Eighty-four OTUs (representing 0.04% of the total number of sequences) were removed from analysis due to an alignment length of <80%. Hidden state prediction was performed with the maximum parsimony method with MetaCyc EC-Numbers. OTUs with a nearest sequenced taxon index >0.2 were excluded from the analysis to improve the accuracy of prediction. Based on this threshold, 60.6% OTUs were kept for functional prediction, representing 72.7% of the total number of sequences. For each sample, the abundance of MetaCyc pathways was predicted and normalized by the total abundance of all pathways.

2.13 | Evaluation of sulfide concentrations in colonic contents

Sulfide concentrations were evaluated by adapting a protocol from Strocchi et al.²⁴ After homogenization in deoxygenated PBS, colonic content was diluted 1:10 (volume/volume) in deoxygenated water. Five hundred microliters of zinc acetate 654 mM (383317, Sigma-Aldrich) were added to 1.5 mL of the latter homogenate. The reagent was prepared by diluting N,N-dimethyl-p-phenylenediamine sulfate (28.5 mM, 186384, Sigma-Aldrich), ferric chloride (36.7 mM, 236489, Sigma-Aldrich) in 50% hydrochloric acid (300 mL). Each homogenate was incubated with a solution containing the reagent, 327 mM zinc acetate, and 50% hydrochloric acid for 20 min at RT. Samples were then centrifuged at 12 000g, 3 min, and the absorbance of the supernatants was read at 670 nm. Several concentrations of sodium sulfide (0.2 μ M to 1 mM) diluted in the same reactive solution were used to generate a standard curve and estimate sulfide concentration. Results were normalized by mg of colonic content.

2.14 | Culture of intestinal organoids and extracellular flux analysis

Crypt colon mouse C57BL/6JOLA Hsd were obtained following the protocol described above. The EDTA/HBSS solution was supplemented with 10 μ M Y27632

(dihydrochloride, Peprotech 1293823) and penicillin/streptomycin (PS) 1%. The pellet of colonic crypts obtained after a 5 min centrifugation at 200g was resuspended in DMEM/F12 (12634010, Gibco) supplemented with 1% PS and centrifuged at 200g. Isolated colonic crypts were embedded in 20 μ L Matrigel and seeded on a 48-well plate (750 crypts/well) and cultured in proliferative medium (Wnt 3A, R-Spondin, Noggin conditioned medium)/(DMEM F12, 50/50, v/v), 15% (FBS, 1% PS) at 37°C, under 10% humidified CO₂ with Y-27632 10 μ M added in the medium to avoid anoikis for the first 24 h. At day 5, organoids were harvested by adding 0.5 mL Tryple Express for 5 min before breaking them by pipetting up and down four times. Then, organoids were rinsed with cold ADF and centrifuged at 200g. Organoid suspension (50 μ L) dissolved in their medium (50 organoids/well) were seeded in precoated matrigel plate Xfp with 10 μ L of 10% Matrigel/Seahorse Medium (DMEM XF medium HCO₃⁻-free modified pH 7.4 containing 25 mM glucose, 2 mM glutamine, 1 mM pyruvate). After solidification of Matrigel at 37°C for 30 min, organoids were treated or not with Na₂S 500 μ M dissolved in a proliferative medium for 48 h. The proliferative medium was changed each morning and evening in order to maintain the H₂S concentration close to the setpoint concentration. OCR and ECAR were determined by Seahorse extracellular XFp Flux Analysis. Before the run, plates and cartridges were prepared following the same protocol as for isolated colonic crypts. Three measurement cycles of OCR and ECAR were performed without any exogen agent to determine basal respiration, in the presence of oligomycin (1.5 μ M), FCCP (1 μ M), and antimycin A/rotenone (0.5 μ M). Cycles consisted of 3 min mix, 2 min wait, and 3 min of measurements after each injection. At the end of the assay, results were normalized by measuring the Hoechst fluorescence intensity of organoids.

2.15 | Measure of mitochondrial complex IV activity using the Seahorse technology

Mitochondria from mouse colonic crypts were isolated using a protocol adapted from Frezza et al.²⁵ Briefly, colonic crypts were isolated as described earlier. Pellet was resuspended in 1 mL of mitochondrial isolation buffer containing sucrose (70 mM, S-8501, Sigma-Aldrich), D-mannitol (210 mM, M9546, Sigma-Aldrich), HEPES (2 mM), and ethylene glycol-bis(β -aminoethyl ether)-N,N,N',N'-tetraacetic acid (EGTA, 1 mM E-4370, Sigma-Aldrich), all diluted in water at pH 7.2. The suspension was maintained in ice and homogenized using a dounce. Homogenized suspension was then centrifuged at 700g for 10 min at 4°C. The resulting supernatant containing

mitochondria was then collected and centrifuged at 8000g for 10 min at 4°C. The pellet, considered isolated mitochondria, was resuspended into 1 mL of mitochondrial assay solution, consisting of sucrose (70 mM), D-mannitol (220 mM), KH₂PO₄ (10 mM, P5655, Sigma-Aldrich), MgCl₂ (5 mM, M2670, Sigma-Aldrich), HEPES (2 mM), and EGTA (1 mM) diluted in water pH 7.2. Mitochondria were then seeded onto Seahorse 24-well plate which was then centrifuged at 2000g for 20 min at 4°C. An additional 450 μ L of mitochondrial assay solution was added to each well and the run was launched. OCR was measured in response to ADP (4 mM), Na₂S (or mitochondrial assay solution as control), TMPD (500 μ M, 87890 Sigma-Aldrich/2 mM, A5960, Sigma-Aldrich), which reduces cytochrome c and thus activates complex IV, and potassium cyanide (KCN, 2 mM, 60178, Sigma-Aldrich), which blocks complex IV activity and allow to determine its own activity. Data were normalized by mg of proteins per well using the BCA protein assay kit (23225, ThermoFisher Scientific).

2.16 | Statistical analysis

Data are represented as mean \pm SEM. Shapiro–Wilk normality test was performed on each data set, followed by a parametric test (Unpaired *t* test) between CTRL and DIO mice, if both data sets followed a normal distribution, or a nonparametric test (Mann–Whitney test) otherwise. Data from organoids were analyzed using unpaired *t* test. A two-way ANOVA was used to determine the effect of diet and time on FD4 flux through mouse colon mounted in a Ussing chamber. PERMANOVA was performed on data from principal coordinates analysis, based on Jaccard distances, to determine if bacterial populations were different between groups. Statistical analysis and graphs were performed on GraphPad Prism version 8.0.2. The PLS-DA was performed with the mixOmics package (6.20.0) in R (4.2.0). Univariate analyses of metabolite relative quantifications and of the relative abundances of microbiota predicted functions were performed nonparametric Kruskal–Wallis test in R. The obtained *p* values were adjusted for multiple comparisons using the false discovery rate procedure. A *p* value of $\leq .05$ was considered significant.

3 | RESULTS

3.1 | Characterization of diet-induced obesity

DIO mice that were fed an obesogenic diet for 22 weeks displayed a 43% body weight increase compared with CTRL

mice (CTRL: 32.5 ± 0.9 vs. DIO: 46.4 ± 1.7 g, $p < .001$) and a marked visceral adiposity index (CTRL: 2.2 ± 0.3 vs. DIO: $6.7 \pm 0.4\%$, $p < .001$). DIO phenotype was also characterized by increased serum concentrations of total cholesterol (CTRL: 2.4 ± 0.3 vs. DIO: 3.6 ± 0.8 mmol/L, $p < .001$) and triglycerides (CTRL: 0.8 ± 0.1 vs. DIO: 1.3 ± 0.2 mmol/L, $p = .002$).

3.2 | Colonic paracellular permeability is increased in DIO mice in association with endotoxemia

FITC-Dextran (FD4) passage through the colonic mucosa from DIO mice was significantly higher than in CTRL mice, indicating an increase in colonic paracellular permeability (Figure 1A). Moreover, gene expressions of *Tjp1* and *Ocln*, encoding tight junction proteins, were decreased by 20% in colonic crypts from DIO mice compared to CTRL mice (Figure 1B). The concentration of circulating LBP was higher in DIO than in CTRL mice (Figure 1C), suggesting metabolic endotoxemia. Furthermore, mRNA relative expression of the stem-cell marker *Lgr5* was higher in isolated crypts from DIO mice, whereas, in contrast,

the expression of the mature colonocyte marker *Krt20* was decreased by obesogenic diet (Figure 1D), suggesting a less mature phenotype of CEC from DIO mice.

3.3 | DIO induces mitochondrial dysfunction of colonic crypts marked by decreased basal and maximal respirations as well as ATP production-linked respiration

To assess the mitochondrial function of colonic crypts, the oxygen consumption rate (OCR) and extracellular acidification rate (ECAR) of isolated colonic crypts from CTRL and DIO mice were measured using the Seahorse technology (Figure 2A). Basal respiration of isolated colonic crypts from DIO mice was twofold lower than in CTRL mice (Figure 2B). Similarly, maximal respiration, measured after the injection of the protonophore carbonyl cyanide-4-phenylhydrazone (FCCP) was reduced in isolated crypts from DIO compared with CTRL mice (Figure 2C). ATP production-linked respiration of isolated colonic crypts was also lower in DIO mice (Figure 2D), suggesting an impairment of ATP production in both basal and stressed

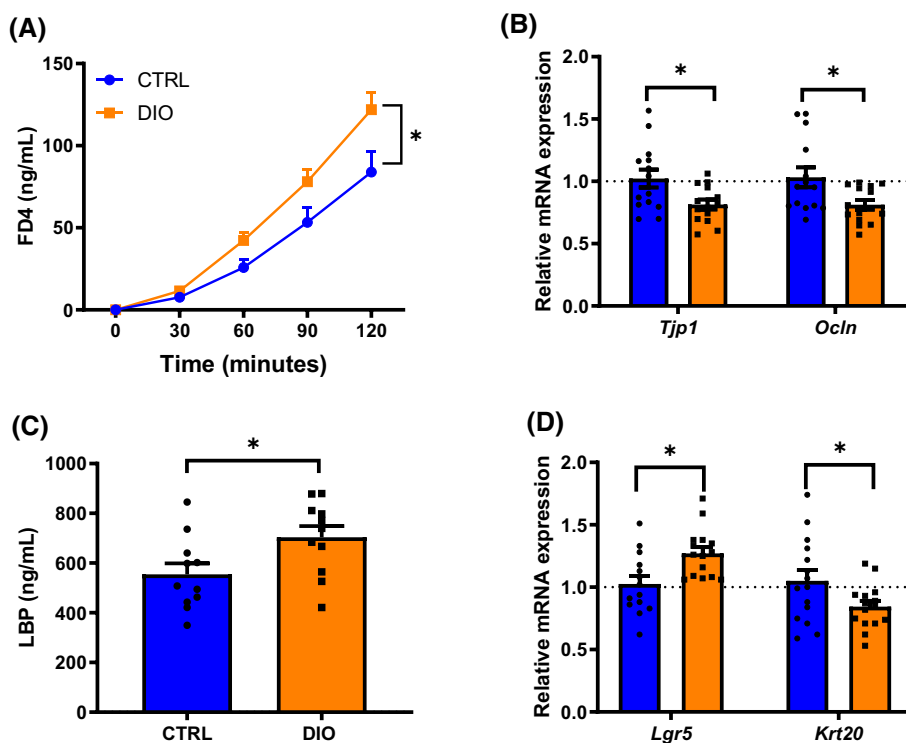


FIGURE 1 Obesogenic diet feeding increases the paracellular permeability of mouse colon and modulates colonic crypt maturation. (A) FITC-dextran 4000 kDa (FD4) flux across mouse colonic mucosa mounted in Ussing chambers ($n = 12$ for CTRL and WD). (B) Relative mRNA expression of tight junction protein of mouse colonic crypts ($n = 15$ for CTRL and DIO). (C) Lipopolysaccharide-binding protein (LBP) concentration in serum samples ($n = 11$ for CTRL and DIO). (D) Relative mRNA expression of *Lgr5*, a marker of stem cells, and *Krt20*, for differentiated colonocytes, in mouse colonic crypts ($n = 15$ for CTRL and DIO). Values are represented as means \pm SEM. Significant differences are represented as * $p < .05$ versus CTRL.

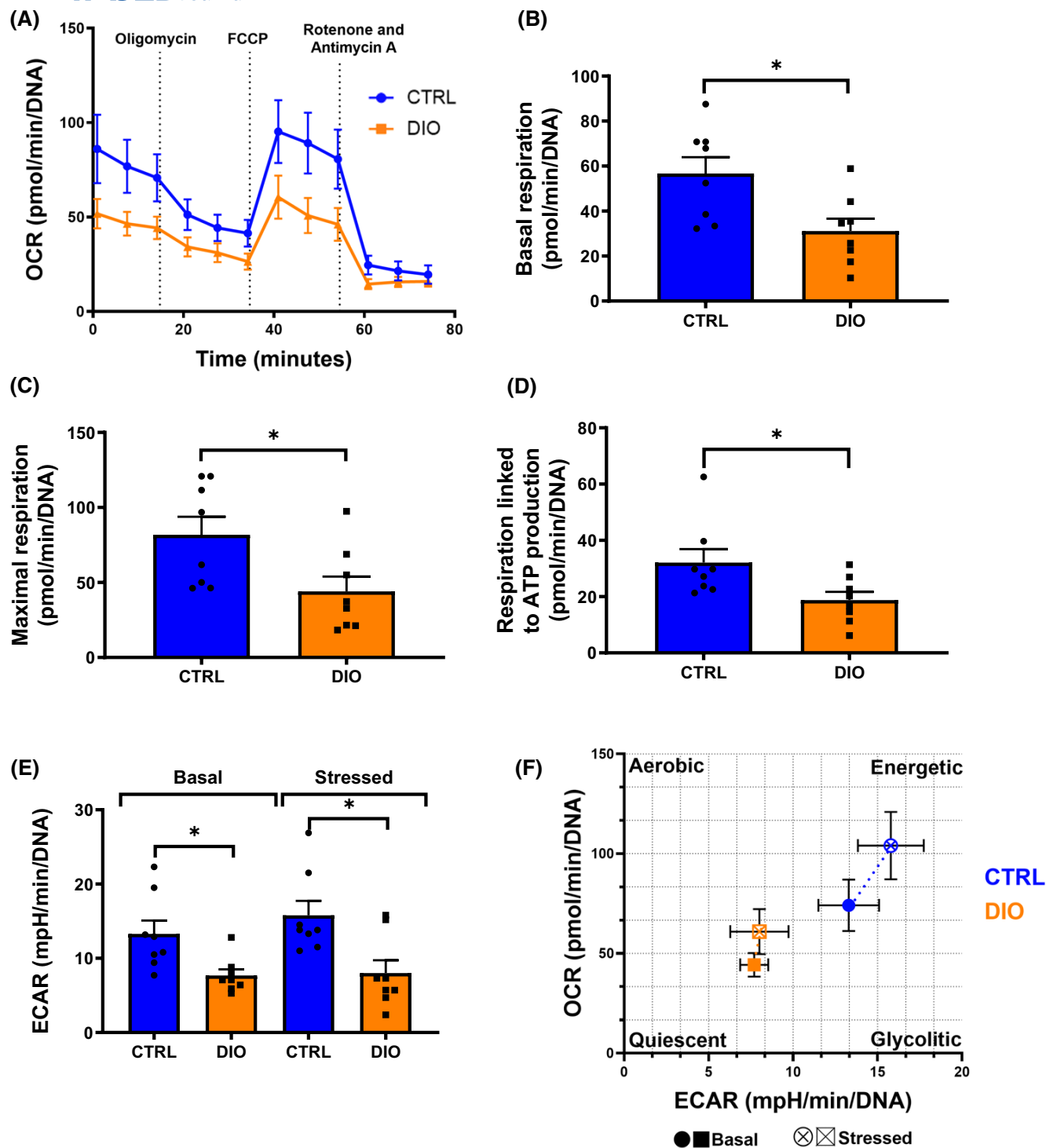


FIGURE 2 Obesogenic diet feeding induces mouse colonic crypt mitochondrial dysfunction. (A) Oxygen consumption rates (OCR) of mouse colonic crypts after sequential injection of oligomycin, FCCP, and antimycin A with rotenone. (B) Basal respiration, (C) maximal respiration, (D) respiration linked to ATP production. (E) Extracellular acidification rates (ECAR) at basal and stressed states. (F) Energy map of colonic crypts in basal (solid circle) or stressed (open circle) conditions obtained from OCR and ECAR. Values are means \pm SEM. Significant differences are represented as * $p \leq .05$ versus CTRL ($n = 8$ for CTRL and DIO).

conditions. Glycolysis was evaluated by the ECAR measures which were lower in colonic crypts from DIO mice compared with those from CTRL, in both basal conditions and under metabolic stress obtained by injection of FCCP

(Figure 2E). Moreover, although the relative mRNA expression of *Phosphofructokinase 1* and *Pyruvate Kinase M2*, encoding for enzymes of glycolysis, was unmodified by DIO, the expression of *Hexokinase 1*, the enzyme that

initiates glycolysis, was diminished by 20% in colonic crypts from DIO mice (Table S3). Consistent with the lower basal and maximal respirations and the lower ECAR of isolated colonic crypts from DIO mice compared with CTRL, metabolic phenotype showed a lower metabolic potential in colonic crypts from DIO mice in both basal and stressed states compared to CTRL mice (Figure 2F).

3.4 | Mitochondrial dynamics of colonic crypts is not altered by DIO

The mitochondrial dysfunction of isolated colonic crypts observed in DIO mice could reflect alterations of mitochondrial dynamics that would modulate the number of mitochondria in CEC. Yet, mRNA expressions of genes involved in mitochondrial biogenesis regulation, fusion,

and fission in colonic crypts were similar between groups (Figure 3A,B). Relative quantification of mtDNA showed similar contents between groups suggesting equivalent mitochondrial mass in isolated crypts regardless of the diet (Figure 3C).

3.5 | DIO decreases *CoxIV* expression of colonic crypts

We next evaluated whether mitochondrial oxidative capacity in colonic crypts from DIO mice was impaired. While obesogenic diet consumption did not modify gene expression of subunits from mitochondrial complexes I, II, and V in isolated colonic crypts, *CoxIV* expression was 18% lower in isolated colonic crypts from DIO mice compared with CTRL mice (Figure 3D).

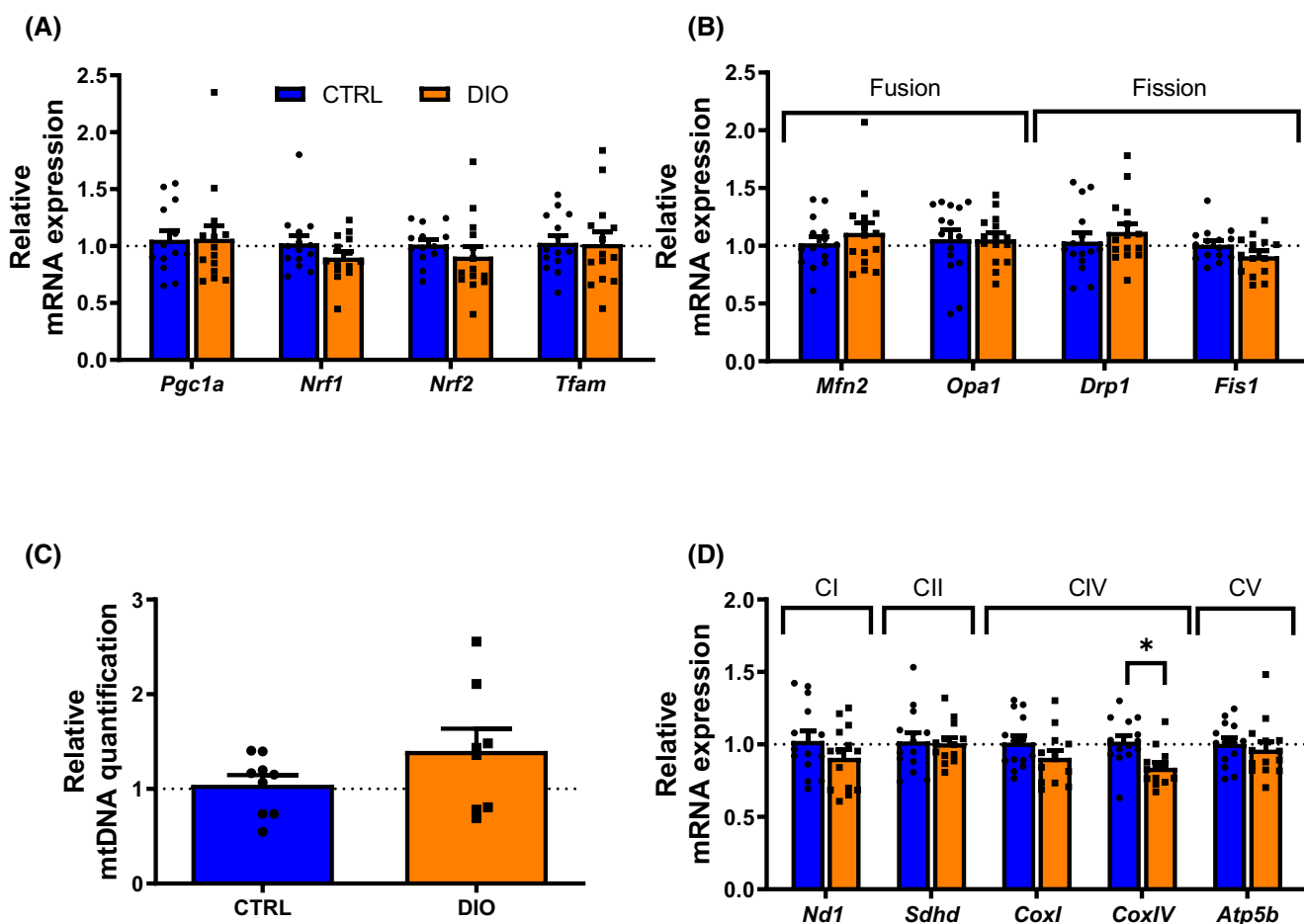


FIGURE 3 Mitochondrial dynamics of colonic crypts from mice is unaltered by DIO while *CoxIV* expression is diminished. Relative mRNA expression of genes encoding (A) mitochondrial biogenesis regulators and (B) targets of mitochondrial fusion and fission ($n = 15$ for CTRL and DIO). (C) Evaluation of mtDNA content normalized to nuclear DNA ($n = 9$ for CTRL and DIO). (D) Relative mRNA expression of genes encoding subunits of ETC complexes: *Nd1* of mitochondrial NADH dehydrogenase, *Sdhb* of Succinate dehydrogenase, *CoxI* and *CoxIV* of cytochrome c oxidase, and *Atp5b* of ATP synthase ($n = 15$ for CTRL and DIO). Abbreviations: CI, complex I; CII, complex II; CIII, complex III; CIV, Complex IV CV, complex V. Values are means \pm SEM. Significant differences are represented as * $p < .05$ versus CTRL.

3.6 | Fatty acids are increased in the colonic content from DIO mice, but they are not more absorbed or β -oxidized by colonic crypts

We next wanted to clarify whether enhanced dietary fatty acid metabolism of isolated crypts was responsible for oxidative stress and subsequent alteration of mitochondrial function. Fatty acid concentrations in the caecal content from DIO mice were 4.5-fold higher compared with that of CTRL (Figure 4A). The relative concentration of glycerol was also higher in the colon from DIO mice (Table S1) and could be related to a higher concentration of triglycerides. Yet, gene expression of the fatty acid transporters *Cd36*, *Fatp4*, and *Cav1* was similar in colonic crypts from both groups (Figure 4B). Moreover, colonic crypts from DIO mice displayed equivalent fatty acid concentrations compared with CTRL mice (Figure 4C). Hence, [U - ^{14}C] palmitic acid β -oxidation capacity was similar in both groups (Figure 4D). We next evaluated if there was any sign of oxidative stress in isolated crypts provoked by DIO.

mtROS and peroxides were measured, respectively, with MitoSOX and H_2DCFDA dyes in isolated colonic crypts. No significant difference in ROS detection was observed between groups (Table 1). Moreover, the expression of genes coding enzymes involved in pro- and antioxidant machineries was similar in isolated colonic crypts from DIO and CTRL mice (Table 1). Taken together, these results dismissed the hypothesis of oxidative stress-induced mitochondrial dysfunction through enhanced dietary fatty acid catabolism in isolated crypts from DIO mice.

3.7 | DIO induces colonic microbiota dysbiosis and increases the relative abundance of Desulfovibrionaceae

We next hypothesized that the mitochondrial dysfunction observed in DIO mouse colonic crypts could be due to alterations in microbiota composition or activities. Thus, the colonic microbiota was characterized in both groups. Principal coordinates analysis, based on Jaccard

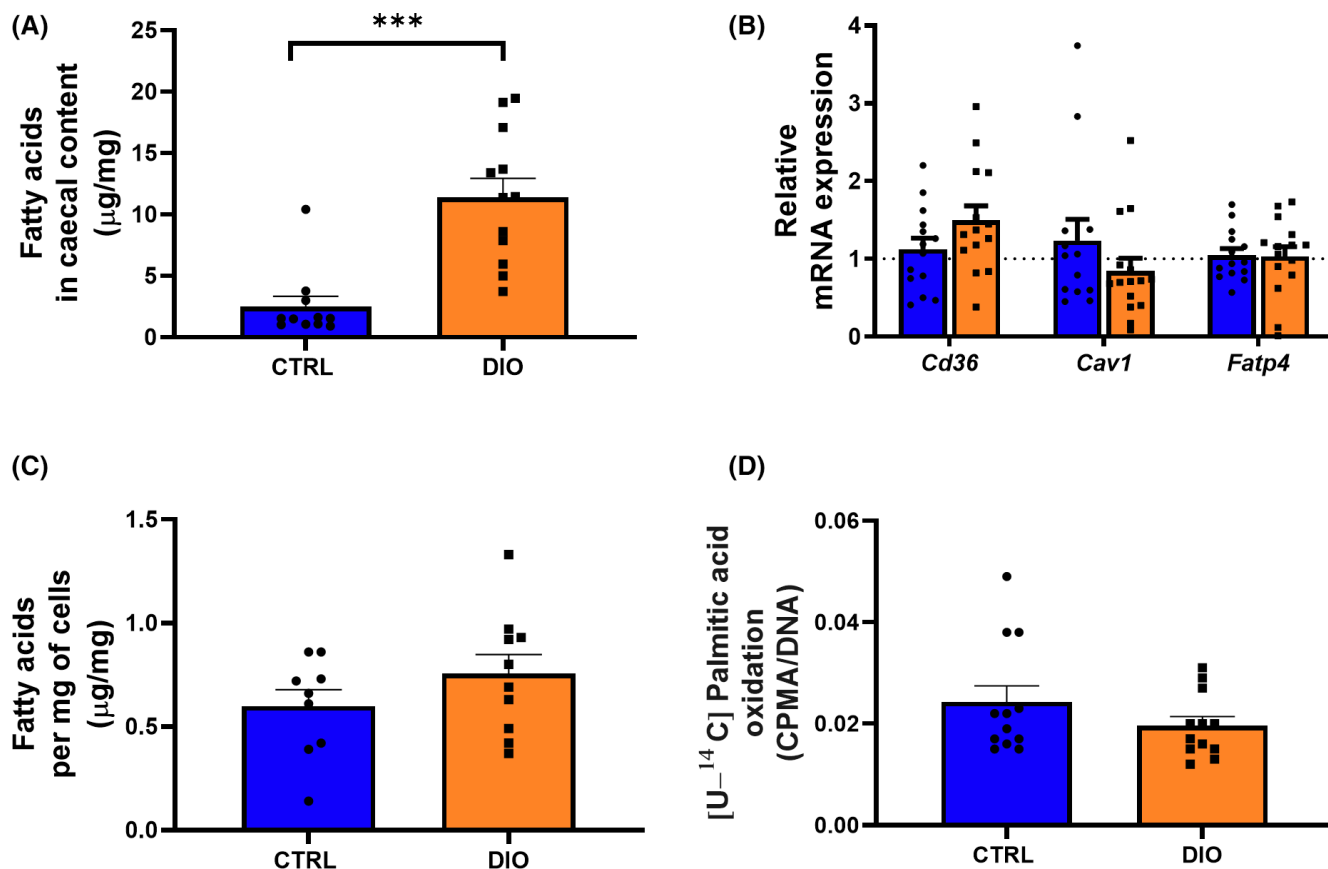


FIGURE 4 DIO does not enhance the fatty acid metabolism of mouse colonic crypts. (A) Quantification of total fatty acids in caecal content by GC-MS ($n = 10$ for CTRL and $n = 12$ for DIO). (B) Relative mRNA expression of fatty acid transporters in colonic crypts ($n = 15$ for CTRL and DIO). (C) Quantification of total fatty acids in colonic crypts by GC-MS ($n = 9$ for CTRL and $n = 10$ for DIO). (D) Measurement of [U - ^{14}C] palmitic acid oxidation in colonic crypts ($n = 12$ for CTRL and DIO). Values are means \pm SEM. Significant differences are represented as *** $p < .001$ versus CTRL.

TABLE 1 Gene expression of pro- and antioxidant machinery enzymes and ROS detection in isolated colonic crypts from mice.

		CTRL	DIO	p value
Pro-oxidant	<i>Duox1</i>	1.34 ± 0.4	1.22 ± 0.5	.50
	<i>Duox2</i>	1.07 ± 0.4	0.98 ± 0.5	.98
Antioxidant	<i>Gpx2</i>	1.02 ± 0.2	1.08 ± 0.3	.36
	<i>Nqo1</i>	1.01 ± 0.2	1.07 ± 0.3	.42
	<i>Gsr</i>	1.05 ± 0.2	0.90 ± 0.2	.39
	<i>Sod1</i>	1.05 ± 0.2	1.01 ± 0.4	.16
	<i>Cat</i>	1.02 ± 0.2	1.02 ± 0.2	.08
	<i>Sirt3</i>	1.02 ± 0.2	0.97 ± 0.2	.08
	<i>Sod2</i>	1.02 ± 0.2	0.90 ± 0.1	.22
ROS detection	mtROS	100.0 ± 7.3	124.5 ± 68.9	.28
	Peroxides	100.0 ± 10.4	90.9 ± 33.2	.64

distances, revealed that the colonic microbiota was different between the two groups (Figure 5A, PERMANOVA $p < .001$). Colonic microbiota from DIO mice was characterized by reduced richness (number of observed OTUs) (Figure 5B). Regarding phyla relative abundance (Figure 5C), while the one of Actinobacteria was significantly lower in the colon of DIO mice compared with that of CTRL mice (19.5% vs. 2.5% for WD, $p = .04$), Proteobacteria relative abundance was three times greater in the colonic lumen of DIO mice (3.9% vs. 11.8%, $p < .005$) which was mostly driven by high proportions of Desulfovibrionaceae (Figure 5D). Within this family, an unknown genus was far more abundant in DIO mice colonic lumen as well as *Bilophila* (Figure 5E).

3.8 | Relative concentrations of short-chain fatty acids in the colonic content are not modified by DIO

Since gut microbiota-derived short-chain fatty acids (SCFA), notably butyrate, are major energetic fuels for CECs, we evaluated if the dysbiosis observed in DIO mice led to changes in SCFA luminal concentrations. NMR-based metabolomics of colonic content revealed that the relative concentrations of butyrate (CTRL: 100.0 ± 11.3% vs. DIO: 91.9 ± 6.8%), propionate (CTRL: 100 ± 22.3% vs. DIO: 94.4 ± 14.3%), and acetate (CTRL: 100.0 ± 15.9% vs. DIO: 85.8 ± 8.3%) were equivalent in both groups. The relative concentrations of other metabolites identified in the colonic luminal environment are presented in Table S1.

3.9 | DIO induces a gut microbiota metabolic shift toward sulfide production

We next used PICRUSt2 to predict functional pathways in the colonic microbiota of CTRL and DIO mice

(Table S2). The relative abundance of the sulfate reduction pathway (SO4ASSIM-PWY) was increased in the gut microbiota of DIO mice (Figure 6A). Indeed, within the Desulfovibrionaceae family, *Desulfovibrio* spp. produce hydrogen sulfide from sulfate and cysteine while *Bilophila wadsworthia* is known to produce H₂S from taurine degradation and sulfite.²⁶ The relative concentration of total bile acids evaluated by NMR was increased by 33% in the colonic lumen of DIO mice (Figure 6B). In contrast, the relative concentration of taurine in the colon content was not different between groups (Table S1). Furthermore, sulfide concentration in the colonic content of DIO mice was significantly increased compared with CTRL ones (Figure 6C). Expression of gene encoding the mitochondrial H₂S detoxification machinery revealed that *Sqor* was diminished by 15% in isolated colonic crypts from DIO mice, whereas *Ethel* and *Tst* expressions were not modified by the diet (Figure 6D).

3.10 | Another mouse model of DIO with lower lipid level on a shorter time reproduces the dysbiosis-related mitochondrial dysfunction of colonic crypts

In another mouse model of DIO, fed for 12 weeks with a western diet (WD) characterized by lower lipid content (45% kcal derived from fat), we found that the colon from WD mice was also characterized by a dysbiosis marked by increased abundance of Desulfovibrionaceae, especially *Bilophila*, as well as higher concentrations of bile acids in the colonic content. Mitochondrial basal respiration of isolated colonic crypts was also lower in WD mice compared with CTRL (Figure S2). Overall, these data suggested that sulfide produced from Desulfovibrionaceae through bacterial conversion of sulfate or taurine associated with bile acids may impair mitochondrial function of colonic crypts from mice fed high-fat diets.

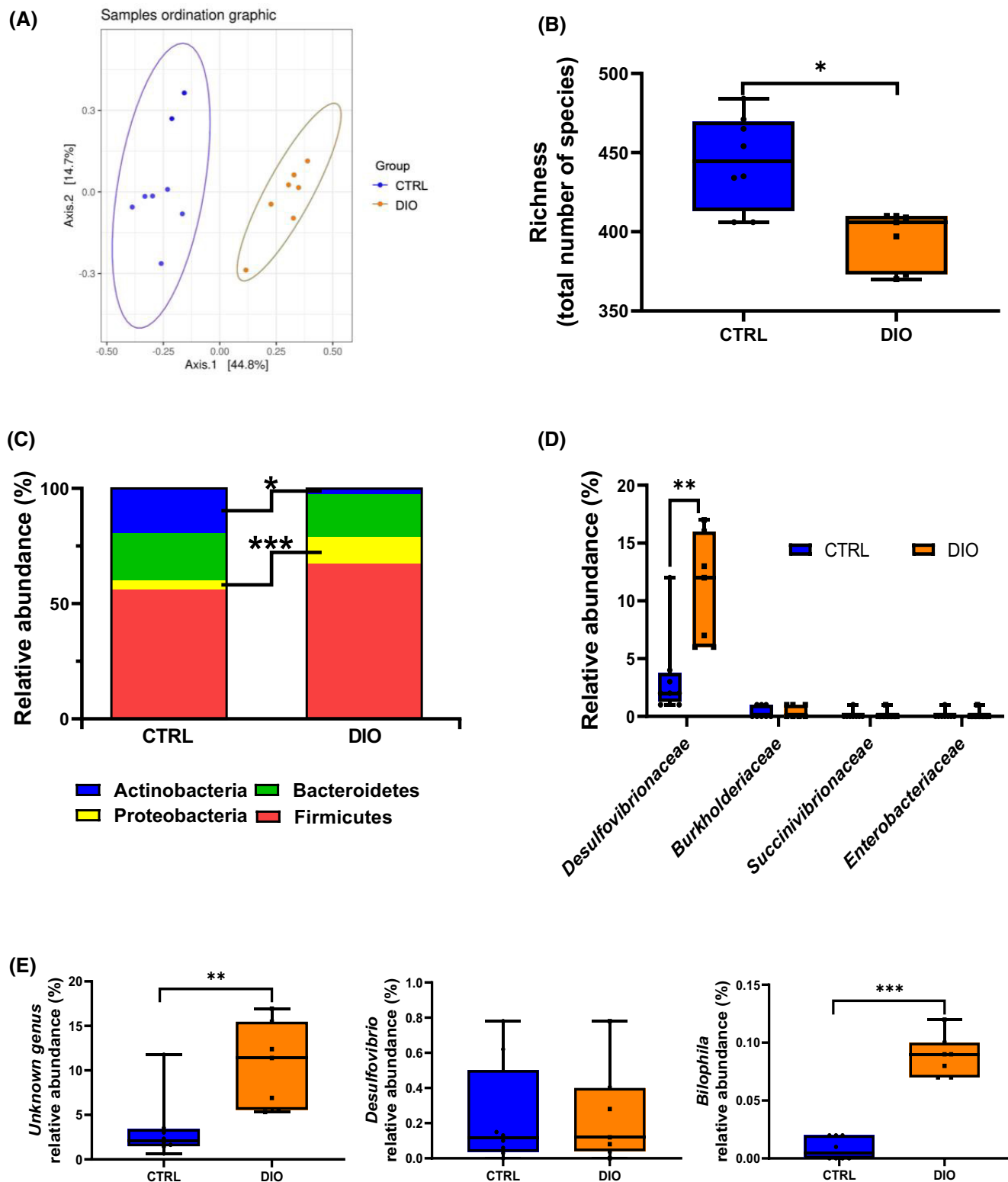


FIGURE 5 DIO induces gut microbiota dysbiosis favoring the growth of sulfur-reducing bacteria. Microbiota analyses were performed from 16S rRNA gene amplicon sequencing of colonic content from CTRL and DIO mice showing (A) β -diversity, (B) richness, (C) relative abundance of the four main phyla, (D) families from the Proteobacteria phylum, and (E) genera from the Desulfovibrionaceae family. Values in box plots are minimum to maximum with a line at median ($n = 8$ for CTRL and $n = 7$ for DIO). Significant differences are represented as $*p \leq .05$, $**p \leq .01$, $***p \leq .001$ versus CTRL.

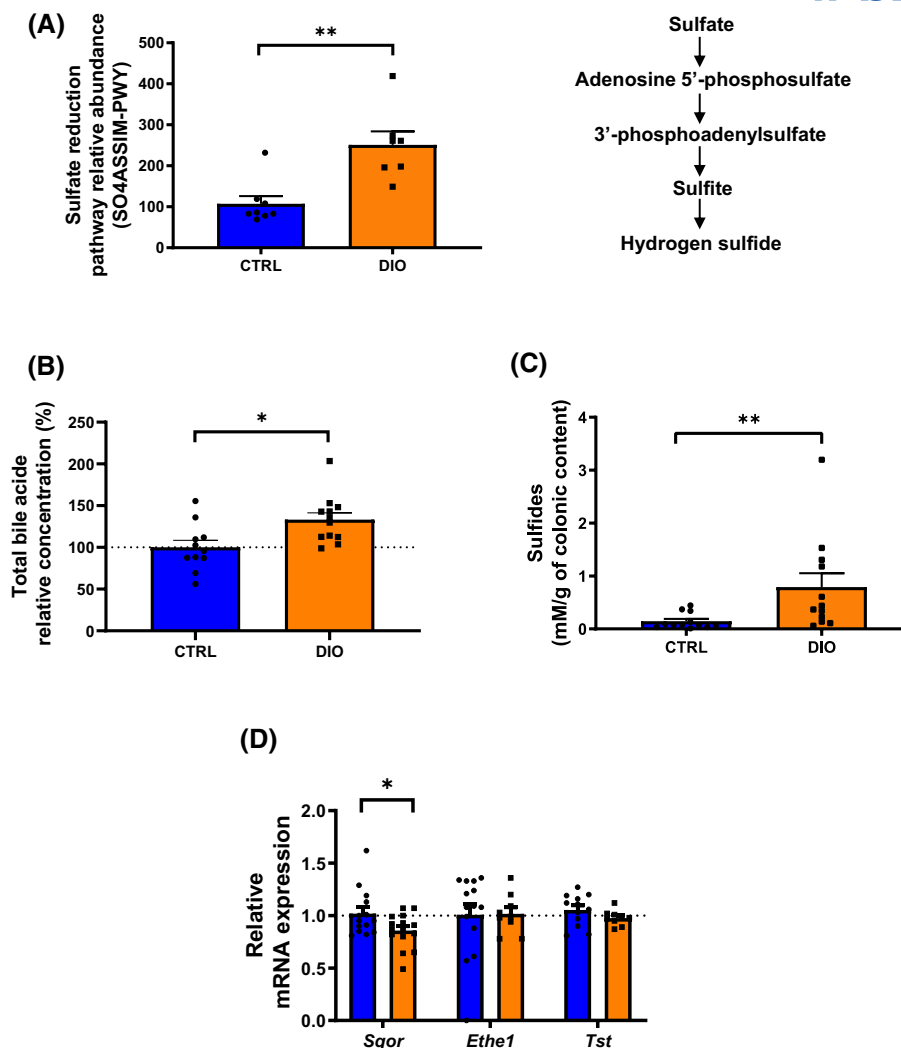


FIGURE 6 DIO enhances sulfide production through bacterial pathways related to sulfate reduction and increased bile acid concentration. (A) Relative abundance in the colonic microbiota of the predicted pathway - sulfate reduction “SO4ASSIM-PWY” ($n = 8$ for CTRL and $n = 7$ for DIO). (B) Relative concentration of bile acids in colonic content detected by H^1 -NMR ($n = 11$ for CTRL and $n = 12$ for DIO). (C) Sulfide concentrations in colonic contents ($n = 12$ for CTRL and $n = 12$ for DIO). (D) Relative mRNA expression of the mitochondrial hydrogen sulfide detoxification enzymes in colonic crypts ($n = 15$ for CTRL and DIO). Values are means \pm SEM. Significant differences are represented as $*p \leq .05$, $**p \leq .01$, $***p \leq .001$ versus CTRL.

3.11 | Chronic exposure of murine colonic organoids to sodium sulfide elicits a mitochondrial dysfunction similar to that observed in vivo

To evaluate the potential deleterious effect of chronic sulfide exposure on CEC mitochondria, organoids from mouse colon were treated for 48 h with 500 μ M sodium sulfide (Na_2S), a sulfide donor. Mitochondrial function of these organoids was evaluated via the Seahorse technology (Figure 7A). Chronic treatment with Na_2S impaired basal respiration (Figure 7B) as well as maximal respiration (Figure 7C), compared with that from untreated

organoids. Respiration linked to ATP synthesis also seemed diminished by the treatment, although differences between the Na_2S -treated and the untreated organoids were not significant (Figure 7D, $p = .06$). Moreover, while the global metabolic phenotype of organoids treated with Na_2S was quiescent at the basal state, it seemed to shift toward a more glycolytic phenotype in a situation of metabolic stress (Figure 7E) although the difference between ECAR at basal and stressed states was not significant in treated organoids (Figure 7F). Interestingly, chronic exposure to 200 μ M Na_2S did not elicit defects of mitochondrial bioenergetics or glycolysis of mouse colon organoids (Figure S3).

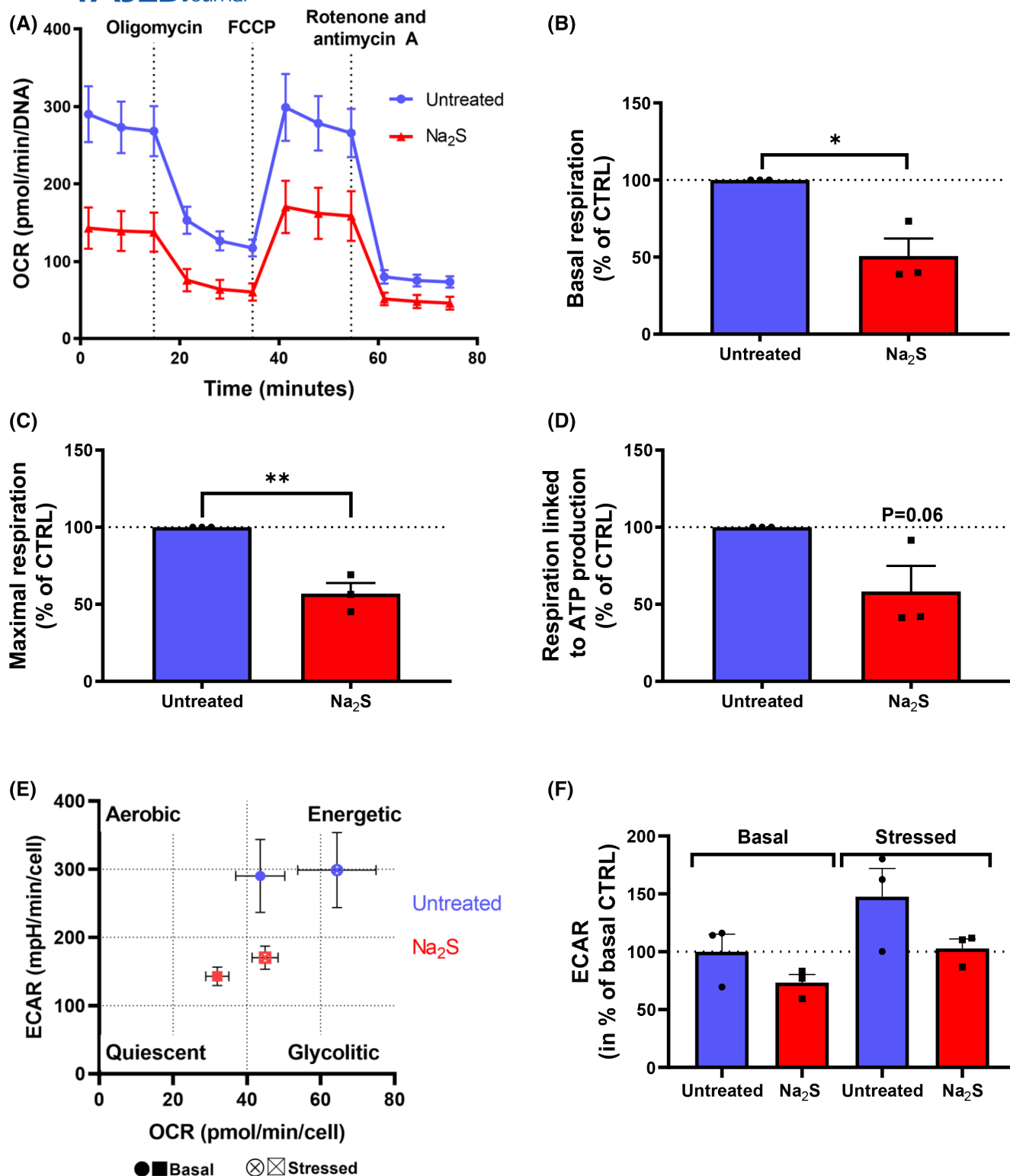


FIGURE 7 Chronic treatment with sodium sulfide (Na_2S) elicits CEC mitochondrial dysfunction in murine organoids similar to that observed in DIO mice. (A) OCR of murine colonic organoids after 48 h treatment with 500 μM Na_2S . Sequential injections were oligomycin, FCCP, and antimycin A with rotenone. (B) Basal respiration, (C) maximal respiration, (D) respiration linked to ATP production of murine colonic organoids represented in the percentage of untreated organoids. (E) Energy map of untreated and Na_2S -treated organoids. (F) ECAR of murine colonic organoids expressed in percentage of the untreated condition at basal state. Values are means \pm SEM. Significant differences are represented as * $p \leq .05$, ** $p \leq .01$, *** $p \leq .001$ versus CTRL ($n = 3$ for untreated and Na_2S -treated organoids).

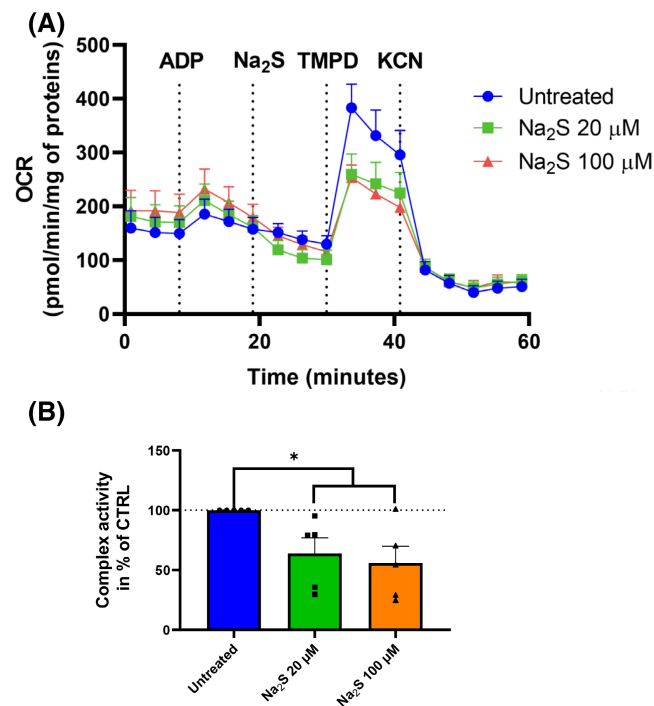


FIGURE 8 Acute exposure with Na₂S of isolated mitochondria from mouse CEC diminishes cytochrome c oxidase activity. (A) OCR of isolated mitochondria from CEC of mice. (B) Cytochrome c oxidase activity in the percentage of the untreated condition. Values are means \pm SEM. Significant differences are represented as * p < .05 versus CTRL (n = 5 mice).

3.12 | Acute exposure of isolated mitochondria from mouse colonic crypts to sodium sulfide decreases complex IV activity

Finally, we evaluated whether the activity of complex IV, which gene expression was reduced in isolated crypts from DIO mice compared with CTRL, was affected by sulfide. Mitochondria were isolated from colonic crypts of mouse that had received the CTRL diet for 2 weeks and complex IV activity was assayed in the presence or absence of Na₂S. An increase in the respiration rate following ADP injection confirmed that oxidative phosphorylation of isolated mitochondria was functional (Figure 8A). Acute treatment of isolated mitochondria with Na₂S elicited a decrease in OCR after N,N,N',N'-tetramethyl-p-phenylenediamine dihydrochloride (TMPD) injection, indicating a lower cytochrome c oxidase activity, regardless of the Na₂S concentration (Figure 8B).

4 | DISCUSSION

In this study, we aimed to better characterize CEC mitochondrial function in DIO and to decipher the underlying

mechanisms of mitochondrial dysfunction if any. Here, we showed that mitochondria from DIO mouse-isolated crypts displayed decreased basal, maximal, and ATP production-linked respirations, indicative of mitochondrial dysfunction. Yet, obesogenic diet consumption did not alter colonic crypt fatty acid metabolism nor elicited oxidative stress but favored sulfide production from Desulfovibrionaceae. In addition, chronic treatment of mouse colonic organoids with sodium sulfide reproduced the *in vivo* mitochondrial alterations, whereas an acute exposure of isolated mitochondria from mouse-isolated crypts to sodium sulfide markedly decreased cytochrome c oxidase activity. Overall, our data support the hypothesis of increased sulfide production by colon dysbiotic microbiota in a context of DIO that impairs mitochondrial complex IV activity leading to mitochondrial dysfunction of CEC, regardless of CEC fatty acid metabolism and oxidative stress.

As obesogenic diets are rich in saturated fatty acids and considering their deleterious impact on mitochondrial function in other tissues^{27,28} and on CEC *in vitro*,^{11,12,14} several authors have hypothesized that enhanced fatty acid oxidation may generate oxidative stress in CEC leading to mitochondrial dysfunction. This organelle is indeed considered the primary target of ROS-induced intracellular damage. In the small intestine, a metabolic shift toward lipid catabolism in enterocytes has been demonstrated in the context of obesity,⁷ both in humans²⁹ and in animal models,³⁰ marked by enhanced lipid storage and increased β -oxidation.³¹ Concomitant to these metabolic alterations, oxidative stress has been observed in the small intestine mucosa from obese mice^{32,33} from which may emerge mitochondrial dysfunction. However, the colon is not known as a site of dietary fatty acid absorption because most of the lipids are absorbed in the small intestine. Nevertheless, hypothesizing that excessive dietary lipids may reach the colon, several authors showed that treating colonocytes with palmitic acid *in vitro* increased ROS generation, altered mitochondrial network, and decreased respiratory rates.^{11,12,14} However, despite the higher abundance of fatty acids in the caecal content from DIO mice, our data on lipid metabolism in CEC neither support the hypothesis of greater absorption and catabolism of fatty acids nor diet-induced oxidative stress in isolated crypts from DIO mice.

In accordance with previous works led on obese humans³⁴ or animals,^{35–37} our study shows that an obesogenic diet enhances the relative abundance of Desulfovibrionaceae. Moreover, in the present study, predictions of microbial metabolic pathways indicated that the capacity of colonic microbiota to metabolize sulfate into H₂S was higher in DIO mice. Bacteria from the Desulfovibrionaceae phylum are known to produce H₂S

through the fermentation of endogenous or diet-derived sulfur-containing amino acids, including *Desulfovibrio* spp, and the reduction of inorganic sulfate into H_2S , for *Desulfovibrio* and *Bilophila wadsworthia*.³⁸ Moreover, *Bilophila wadsworthia* is a bile-tolerant bacteria whose abundance is increased by HFD³⁹ and produces H_2S through taurine degradation.⁴⁰ Bile acids, including sulfated bile acids and taurine-conjugated, are increased in response to high-fat feeding in obese humans⁴¹ and mice.⁴² Besides, bacterial degradation of taurocholic acid in HFD favors *Bilophila wadsworthia* abundance.³⁵ Accordingly, higher concentrations of bile acids were found in the colonic luminal environment of our DIO-fed mice. In mice, taurine-conjugated bile acids are predominant over the glycine-conjugated ones and contrary to humans.⁴³ Hence, most sulfur in DIO mice should arise from bacterial degradation of taurine. Relative abundance of Desulfovibrionaceae is also increased in obese subjects³⁴ and suggests that the existence of a Desulfovibrionaceae-induced mitochondrial dysfunction of CEC may occur in humans as well.

While 22 weeks of DIO in mice induced mitochondrial dysfunction in epithelial cells of isolated crypts, we also showed that feeding mice during 12 weeks with lower amounts of fat (45% in WD vs. 58% kcal derived from lipids in DIO) provoked increased abundance of *Bilophila* and bile acid concentrations associated with reduced basal respiration of isolated crypts from WD mice too. This suggested an association between microbiota-derived sulfide and CEC mitochondrial function.

Although sulfides are difficult to be measured in situ given their volatility, they can approximately be found at concentrations ranging from 0.2 mM to 2.0 mM in the colon.^{44,45} According to their concentration, sulfides can be energetic fuel or metabolic perturbators. Acute exposure of HT-29 Glc^{-/+} to NaHS at concentrations below 20 μ M indeed stimulated O_2 consumption and ATP production, whereas, at concentrations higher than 65 μ M, it inhibited CEC respiration through reduced mitochondrial cytochrome c oxidase activity,⁴⁶ by binding to its heme center.⁴⁷ In the present study, acute exposure of mouse CEC-isolated mitochondria to 100 μ M Na_2S impaired cytochrome c oxidase activity. Surprisingly, at 20 μ M, where sulfides are supposed to stimulate colonocyte respiration,⁴⁶ cytochrome c oxidase activity was also impaired. This is in accordance with a study in rat liver isolated mitochondria showing that sulfides promoted ATP generation and mitochondrial respiration at very low doses (below 3 μ M), whereas it acted already as a metabolic perturbator at 10 μ M.⁴⁸ To assess the effect of H_2S on mouse CEC respiration, we used mouse colonic organoids, which were treated with 500 μ M Na_2S , an intermediate concentration between the sulfide concentration measured in the colon of our DIO mice and those

reported in human colon.⁴⁴ Herein, chronic exposure of organoids to sodium sulfide reproduced the mitochondrial dysfunction observed in vivo in isolated crypts from DIO mice. However, although we and others demonstrated that H_2S is deleterious for the cytochrome c oxidase activity above 20 μ M, we also showed that chronic exposure of mouse colon organoids to 200 μ M Na_2S did not elicit mitochondrial dysfunction. This raises the question of the actual H_2S concentration to which mitochondria from colonocytes are exposed in vitro and in vivo considering its volatility, its diffusion through culture media/lumen and membranes as well as eventual binding with cytosolic compounds. We have to acknowledge that measures of mitochondrial respiration of DIO mouse-isolated colonic crypts or chronically Na_2S -treated colonic organoids with the Seahorse technology were not performed in presence of sulfide. Yet, H_2S impairment of cytochrome c oxidase seems reversible in a dose-dependent manner as shown in vitro in HT-29 after acute exposure to NaHS.⁴⁹ However, others have shown that the H_2S -driven blocking of complex IV, after a rat inhaled H_2S , persisted between the time when mitochondria were isolated from its lung until the complex activity measurement was performed.⁵⁰ Moreover, expression of *CoxIV*, encoding one of the 14 subunits that constitute complex IV, was diminished in DIO mouse colonic crypts, likely contributing to the observed decrease in mitochondrial oxidative capacity. In line with this result, a 24 h exposure in vitro of HT-29 colon cells to 1 mM NaHS diminished the protein expression of complex IV subunits I and II.⁴⁹ Overall, our data strengthen the hypothesis of an H_2S -induced mitochondrial dysfunction involving the complex IV of the ETC in the context of obesogenic diet consumption.

Some authors demonstrated that high-fat feeding in mice resulted in increased intracellular lactate concentrations and decreased pyruvate dehydrogenase activity of CEC^{12,13} which suggested a metabolic shift of CEC toward glycolysis to maintain energetic production while OXPHOS was impaired. In the same line, lactate production was increased in vitro after treating HT-29 cells with 1 mM NaHS for 24 h, indicating increased glycolysis to sustain ATP generation in case of OXPHOS impairment.⁴⁹ However, in our model, ECAR and *Hexokinase1* expression were lower in colonic crypts from DIO mice compared with CTRL ones, suggesting lower glycolysis in DIO mouse-isolated crypts while it remained the same than the control condition in Na_2S -treated colonic organoids. Taken together, our data do not support the hypothesis of a metabolic shift toward glycolysis in the case of sulfide exposure or DIO. Thus, glucose, that can be absorbed from blood circulation by colonocytes, is probably not used as a metabolic substrate by isolated crypts from DIO mice to sustain ATP production. As for SCFA, their

relative concentrations were not modified in the colon of our DIO mice nor in the feces from other models of obese mice⁵¹ while human obesity is often associated with increased fecal concentrations of SCFA, including butyrate.⁵² Because a metabolic shift did not occur toward glycolysis to sustain CEC energetic needs, butyrate oxidation may still occur in colonocytes but could be diminished by the deleterious effect of H₂S on the ETC, leading to decreased ATP production.

In conclusion, we showed here that consumption of an obesogenic diet provoked colon dysbiosis, favoring sulfide production and CEC mitochondrial dysfunction, regardless of CEC lipid metabolism, but likely due to H₂S-driven impairment of cytochrome c oxidase. This CEC energy supply failing could promote the loss of intestinal homeostasis and notably its permeability, aggravating metabolic endotoxemia or even increasing susceptibility to intestinal inflammation.

ACKNOWLEDGEMENT

Authors would like to thank the Get-Plage core facility for 16S sequencing and the ARCHE animal facility. We also thank the Biochemistry Department at the Rennes University Hospital and Manuel Vlach for their technical support.

AUTHOR CONTRIBUTIONS

Annaïg Lan and Gaëlle Boudry supervised the project. Thomas Guerbette, Gaëlle Boudry, and Annaïg Lan conceptualized research and collected data. Thomas Guerbette, Martin Beaumont, Vincent Ciesielski, Jean-Baptiste Perrin, Gaëlle Boudry, and Annaïg Lan analyzed data. Thomas Guerbette, Mireille Andriamihaja, Gaëlle Boudry, and Annaïg Lan performed research. Martin Beaumont and Vincent Rioux developed analytic tools. Thomas Guerbette, Gaëlle Boudry, and Annaïg Lan wrote the paper with the contribution of all co-authors.

FUNDING INFORMATION

TG was partly funded by Region Bretagne (grant no. 300000592).

DISCLOSURES

The authors have stated explicitly that there is no conflict of interest in connection with this article.

DATA AVAILABILITY STATEMENT

16S sequence fasta file of the colonic microbiota data and associated metadata are openly available on *Recherche Data Gouv* at [10.57745/GJXAGJ](https://doi.org/10.57745/GJXAGJ).

ORCID

Thomas Guerbette  <https://orcid.org/0000-0002-7535-1441>

Martin Beaumont  <https://orcid.org/0000-0002-1559-2067>
Mireille Andriamihaja  <https://orcid.org/0000-0001-6322-187X>
Vincent Ciesielski  <https://orcid.org/0009-0004-7783-4414>
Olivier Loréal  <https://orcid.org/0000-0002-7428-3766>
Vincent Rioux  <https://orcid.org/0000-0001-9837-1675>
Gaëlle Boudry  <https://orcid.org/0000-0002-5287-571X>
Annaïg Lan  <https://orcid.org/0000-0003-2044-9377>

REFERENCES

1. Minihane AM, Vinoy S, Russell WR, et al. Low-grade inflammation, diet composition and health: current research evidence and its translation. *Br J Nutr*. 2015;114(7):999-1012.
2. Calder PC, Ahluwalia N, Brouns F, et al. Dietary factors and low-grade inflammation in relation to overweight and obesity. *Br J Nutr*. 2011;106(S3):S1-S78.
3. Hamilton MK, Boudry G, Lemay DG, Raybould HE. Changes in intestinal barrier function and gut microbiota in high-fat diet-fed rats are dynamic and region dependent. *Am J Physiol-Gastrointest Liver Physiol*. 2015;308(10):G840-G851.
4. Cani PD, Possemiers S, Van de Wiele T, et al. Changes in gut microbiota control inflammation in obese mice through a mechanism involving GLP-2-driven improvement of gut permeability. *Gut*. 2009;58(8):1091-1103.
5. Stenman LK, Holma R, Korpela R. High-fat-induced intestinal permeability dysfunction associated with altered fecal bile acids. *World J Gastroenterol*. 2012;18(9):923-929.
6. Genser L, Aguanno D, Soula HA, et al. Increased jejunal permeability in human obesity is revealed by a lipid challenge and is linked to inflammation and type 2 diabetes. *J Pathol*. 2018;246(2):217-230.
7. Guerbette T, Boudry G, Lan A. Mitochondrial function in intestinal epithelium homeostasis and modulation in diet-induced obesity. *Mol Metab*. 2022;63:101546.
8. Wang A, Keita ÅV, Phan V, et al. Targeting mitochondria-derived reactive oxygen species to reduce epithelial barrier dysfunction and colitis. *Am J Pathol*. 2014;184(9):2516-2527.
9. Lewis K, Caldwell J, Phan V, et al. Decreased epithelial barrier function evoked by exposure to metabolic stress and nonpathogenic *E. coli* is enhanced by TNF- α . *Am J Physiol-Gastrointest Liver Physiol*. 2008;294(3):G669-G678.
10. McKay DM, Mancini NL, Shearer J, Shutt T. Perturbed mitochondrial dynamics, an emerging aspect of epithelial-microbe interactions. *Am J Physiol Gastrointest Liver Physiol*. 2020;318(4):G748-G762.
11. Sun Y, Jin C, Zhang X, Jia W, Le J, Ye J. Restoration of GLP-1 secretion by Berberine is associated with protection of colon enterocytes from mitochondrial overheating in diet-induced obese mice. *Nutr Diabetes*. 2018;8:53.
12. Lee JY, Cevallos SA, Byndloss MX, et al. High-fat diet and antibiotics cooperatively impair mitochondrial bioenergetics to trigger Dysbiosis that exacerbates pre-inflammatory bowel disease. *Cell Host Microbe*. 2020;28(2):273-284.
13. Yoo W, Zieba JK, Foegeding NJ, et al. High-fat diet-induced colonocyte dysfunction escalates microbiota-derived trimethylamine N-oxide. *Science*. 2021;373:813-818.
14. Li X, Li X. Obesity promotes experimental colitis by increasing oxidative stress and mitochondrial dysfunction in the colon.

- Inflammation* [Internet]. 2020;43(5):1884-1892. doi:10.1007/s10753-020-01261-6
15. Lone JB, Koh WY, Parry HA, et al. Gut microbiome: microflora association with obesity and obesity-related comorbidities. *Microb Pathog*. 2018;124:266-271.
 16. Ben Fradj S, Nédélec E, Salvi J, et al. Evidence for constitutive microbiota-dependent short-term control of food intake in mice: is there a link with inflammation, oxidative stress, Endotoxemia, and GLP-1? *Antioxid Redox Signal*. 2022;37(4-6):349-369.
 17. Fan YY, Davidson LA, Callaway ES, Wright GA, Safe S, Chapkin RS. A bioassay to measure energy metabolism in mouse colonic crypts, organoids, and sorted stem cells. *Am J Physiol-Gastrointest Liver Physiol*. 2015;309(1):G1-G9.
 18. Drouin G, Catheline D, Guillocheau E, et al. Comparative effects of dietary n-3 docosapentaenoic acid (DPA), DHA and EPA on plasma lipid parameters, oxidative status and fatty acid tissue composition. *J Nutr Biochem*. 2019;63:186-196.
 19. Arnaud AP, Rome V, Richard M, Formal M, David-Le Gall S, Boudry G. Post-natal co-development of the microbiota and gut barrier function follows different paths in the small and large intestine in piglets. *FASEB J*. 2020;34(1):1430-1446.
 20. Beaumont M, Paës C, Mussard E, et al. Gut microbiota derived metabolites contribute to intestinal barrier maturation at the suckling-to-weaning transition. *Gut Microbes*. 2020;11(5):1268-1286.
 21. Lefort G, Liaubet L, Canlet C, et al. ASICS: an R package for a whole analysis workflow of 1D 1H NMR spectra. *Bioinformatics*. 2019;35(21):4356-4363.
 22. Douglas GM, Maffei VJ, Zaneveld JR, et al. PICRUSt2 for prediction of metagenome functions. *Nat Biotechnol*. 2020;38(6):685-688.
 23. Escudié F, Auer L, Bernard M, et al. FROGS: find, rapidly, OTUs with galaxy solution. *Bioinformatics*. 2018;34(8):1287-1294.
 24. Stocchi A, Furne JK, Levitt MD. A modification of the methylene blue method to measure bacterial sulfide production in feces. *J Microbiol Methods*. 1992;15(2):75-82.
 25. Frezza C, Cipolat S, Scorrano L. Organelle isolation: functional mitochondria from mouse liver, muscle and cultured fibroblasts. *Nat Protoc*. 2007;2(2):287-295.
 26. Carbonero F, Benefiel AC, Alizadeh-Ghamsari AH, Gaskins HR. Microbial pathways in colonic sulfur metabolism and links with health and disease. *Front Physiol* [Internet]. 2012 [cited 25 Jan 2021];3:448. <https://www.ncbi.nlm.nih.gov/pmc/articles/PMC3508456/>
 27. Koliaki C, Szendroedi J, Kaul K, et al. Adaptation of hepatic mitochondrial function in humans with non-alcoholic fatty liver is lost in Steatohepatitis. *Cell Metab*. 2015;21(5):739-746.
 28. Wojtczak L, Schönfeld P. Effect of fatty acids on energy coupling processes in mitochondria. *Biochim Biophys Acta BBA - Bioenerg*. 1993;1183(1):41-57.
 29. Tremblay AJ, Lamarche B, Guay V, Charest A, Lemelin V, Couture P. Short-term, high-fat diet increases the expression of key intestinal genes involved in lipoprotein metabolism in healthy men. *Am J Clin Nutr*. 2013;98(1):32-41.
 30. D'Aquila T, Zembroski AS, Buhman KK. Diet induced obesity alters intestinal cytoplasmic lipid droplet morphology and proteome in the postprandial response to dietary fat. *Front Physiol*. 2019;10:180.
 31. Kondo H, Minegishi Y, Komine Y, et al. Differential regulation of intestinal lipid metabolism-related genes in obesity-resistant a/J vs. obesity-prone C57BL/6J mice. *Am J Physiol Endocrinol Metab*. 2006;291(5):E1092-E1099.
 32. Gil-Cardoso K, Ginés I, Pinent M, Ardévol A, Terra X, Blay M. A cafeteria diet triggers intestinal inflammation and oxidative stress in obese rats. *Br J Nutr*. 2017;117(2):218-229.
 33. Qiao Y, Sun J, Ding Y, Le G, Shi Y. Alterations of the gut microbiota in high-fat diet mice is strongly linked to oxidative stress. *Appl Microbiol Biotechnol*. 2013;97(4):1689-1697.
 34. Palmas V, Pisanu S, Madau V, et al. Gut microbiota markers associated with obesity and overweight in Italian adults. *Sci Rep*. 2021;11(1):5532.
 35. Devkota S, Wang Y, Musch M, et al. Dietary fat-induced taurocholic acid production promotes pathobiont and colitis in IL-10^{-/-} mice. *Nature*. 2012;487(7405):104-108.
 36. Zhang C, Zhang M, Wang S, et al. Interactions between gut microbiota, host genetics and diet relevant to development of metabolic syndromes in mice. *ISME J*. 2010;4(2):232-241.
 37. Natividad JM, Lamas B, Pham HP, et al. *Bilophila wadsworthia* aggravates high fat diet induced metabolic dysfunctions in mice. *Nat Commun*. 2018;9(1):2802.
 38. Blachier F, Andriamihaja M, Larraufie P, Ahn E, Lan A, Kim E. Production of hydrogen sulfide by the intestinal microbiota and epithelial cells and consequences for the colonic and rectal mucosa. *Am J Physiol-Gastrointest Liver Physiol*. 2021;320(2):G125-G135.
 39. David LA, Maurice CF, Carmody RN, et al. Diet rapidly and reproducibly alters the human gut microbiome. *Nature*. 2014;505(7484):559-563.
 40. Laue H, Dengler K, Cook AM. Taurine reduction in anaerobic respiration of *Bilophila wadsworthia* RZATAU. *Appl Environ Microbiol*. 1997;63(5):2016-2021.
 41. Ou J, DeLany JP, Zhang M, Sharma S, O'Keefe SJD. Association between low colonic short-chain fatty acids and high bile acids in high colon cancer risk populations. *Nutr Cancer*. 2012;64(1):34-40.
 42. Murakami Y, Tanabe S, Suzuki T. High-fat diet-induced intestinal hyperpermeability is associated with increased bile acids in the large intestine of mice. *J Food Sci*. 2016;81(1):H216-H222.
 43. Li J, Dawson PA. Animal Models to Study Bile Acid Metabolism. *Biochim Biophys Acta Mol Basis*. 2019;1865(5):895-911.
 44. Macfarlane GT, Gibson GR, Cummings JH. Comparison of fermentation reactions in different regions of the human colon. *J Appl Bacteriol*. 1992;72(1):57-64.
 45. Magee EA, Richardson CJ, Hughes R, Cummings JH. Contribution of dietary protein to sulfide production in the large intestine: an in vitro and a controlled feeding study in humans. *Am J Clin Nutr*. 2000;72(6):1488-1494.
 46. Mimoun S, Andriamihaja M, Chaumontet C, et al. Detoxification of H₂S by differentiated colonic epithelial cells: implication of the sulfide oxidizing unit and of the cell respiratory capacity. *Antioxid Redox Signal*. 2012;17(1):1-10.
 47. Hill BC, Woon TC, Nicholls P, Peterson J, Greenwood C, Thomson AJ. Interactions of sulphide and other ligands with cytochrome c oxidase. An electron-paramagnetic-resonance study. *Biochem J*. 1984;224(2):591-600.
 48. Módos K, Coletta C, Erdélyi K, Papapetropoulos A, Szabo C. Intramitochondrial hydrogen sulfide production by 3-mercaptopyruvate sulfurtransferase maintains mitochondrial

- electron flow and supports cellular bioenergetics. *FASEB J*. 2013;27(2):601-611.
49. Leschelle X, Goubern M, Andriamihaja M, et al. Adaptive metabolic response of human colonic epithelial cells to the adverse effects of the luminal compound sulfide. *Biochim Biophys Acta BBA*. 2005;1725(2):201-212.
50. Khan AA, Schuler MM, Prior MG, et al. Effects of hydrogen sulfide exposure on lung mitochondrial respiratory chain enzymes in rats. *Toxicol Appl Pharmacol*. 1990;103(3):482-490.
51. Lu Y, Fan C, Li P, Lu Y, Chang X, Qi K. Short chain fatty acids prevent high-fat-diet-induced obesity in mice by regulating G protein-coupled receptors and gut microbiota. *Sci Rep*. 2016;6(1):37589.
52. Kim KN, Yao Y, Ju SY. Short chain fatty acids and fecal microbiota abundance in humans with obesity: a systematic review and meta-analysis. *Nutrients*. 2019;11(10):2512.

SUPPORTING INFORMATION

Additional supporting information can be found online in the Supporting Information section at the end of this article.

How to cite this article: Guerbette T, Beaumont M, Andriamihaja M, et al. Obesogenic diet leads to luminal overproduction of the complex IV inhibitor H₂S and mitochondrial dysfunction in mouse colonocytes. *The FASEB Journal*. 2023;37:e22853. doi:[10.1096/fj.202201971R](https://doi.org/10.1096/fj.202201971R)